Substituent-Dependent Backward Reaction in Mechanofluorochromism of Dibenzoylmethanato Difluoroboron Derivative

Takehiro Sagawa,[a] Fuyuki Ito,*[a] Atsushi Sakai,[b] Yudai Ogata,[c] Keiji Tanaka[c] and Hiroshi Ikeda[b]

The thermally backward reaction involved in the mechanofluorochromism of dibenzoylmethanatoboron difluoride (BF$_2$DBM) derivatives, accompanied by an amorphous–crystalline phase transition, was quantitatively evaluated based on kinetics and thermodynamics. 10 The kinetics was discussed by evaluation of the effect of temperature on the time-dependent changes of the fluorescence intensity for amorphous samples obtained by mechanical grinding. The thermodynamics was discussed based on data for the amorphous–crystalline phase transition obtained by differential scanning calorimetry. The enthalpy of activation ($\Delta H^{\ddagger}$) of BF$_2$DBM derivatives with MeO groups (**2aBF$_2$**) was larger than that of derivatives with alkyl groups (**2b–** 15 **dBF$_2$**), whereas the entropy of activation ($\Delta S^{\ddagger}$) was smaller than that of derivatives with alkyl groups. It is proposed that the reaction dynamics of **2aBF$_2$** will be governed by rotational motion around the C(methyl)−O bond. Interestingly, the Gibbs energies of activation ($\Delta G^{\ddagger}$) were comparable for the reactions of all members of the BF$_2$DBM series, though $\Delta H^{\ddagger}$ and $\Delta S^{\ddagger}$ were strongly dependent on the identity of the substituent. It is proposed that the substituent-dependent 20 $\Delta S^{\ddagger}$ term is one of the key parameters for understanding the mechanofluorochromism of BF$_2$DBM derivatives associated with the amorphous–crystalline phase transition. These findings will also provide important insights into the process of formation of crystal nuclei in moving from the melted to crystalline state.

Introduction

25 Fluorescence switching in response to external stimuli, namely mechanofluorochromism, is highly interesting as this phenomenon can potentially be exploited for sensor, memory, and security ink applications, etc. Furthermore, fundamental information regarding intermolecular interactions can be 30 garnered from the fluorescence properties of the organic molecular solids that exhibit this phenomenon.[1, 2] The mechanochromic behavior is not a feature of monomeric species, but emerges from assemblies such as crystals, liquid crystals, or amorphous solids.[3-6] Organic molecular solids 35 assembled by relatively weak intermolecular interactions based on van der Waals interactions, such as π–π interactions, hydrogen bonding interactions[7] and aurophilic interactions,[8, 9] exhibit elasticity, which may be significant for modulation of the molecular packing. From another point of view, it is 40 necessary to understand the cooperative interactions in condensed media, where these interactions give rise to tunable optoelectronic properties. The mechanofluorochromic effects of organic solids have been evaluated based on the synthesis of new molecules and their emission properties, emission 45 color changes, crystallography, and thermal properties. The design of molecular structures that exhibit mechanofluorochromism has to be achieved empirically, because fundamental guidelines for judicious design of such architectures have not yet been established.

50 Dibenzoylmethanatoboron difluoride (BF$_2$DBM) derivative exhibits mechanofluorochromism in response to perturbation by a mechanical force.[10-17] BF$_2$DBM derivatives are known for their impressive optical properties, such as their two-photon absorption cross-sections,[18, 19] high fluorescence 55 quantum yield even in the solid state,[20] and multi-fluorescence colors.[12, 21-23] Fraser et al. reported a reversible mechanofluorochromic organic solid based on the 4-*tert*-butyl-4'-methoxydibenzoylmethane (trade name: avobenzone) boron difluoride complex, which exhibits different emission 60 depending on the crystal types.[10] The emission wavelength is significantly red-shifted upon rubbing/smearing the samples. The samples then revert to the original emissive species over time. This is the first finding of thermally backward type (t-type) mechanofluorochromism. There are many substituted 65 BF$_2$DBM complexes with mechanofluorochromic properties that influence their emission color and reaction speed. However, the kinetic and thermodynamic properties of t-type mechanochromic compounds have not been examined.

Information regarding the transition state in the thermally 70 backward reaction, associated with molecular arrangement, is significant for understanding and for designing such reaction systems. For example, Abe et al. recently reported the thermodynamic parameters for the transition state of the photochromic reaction of bridged imidazole dimers to clarify 75 structural changes in the transition state.[24, 25] In the classical nucleation theory, the rate of the crystal formation is considered to follow an Arrhenius-type reaction. Recently, we reported thermodynamic analysis of the thermally backward reaction of BF$_2$DBM derivatives after mechanical 80 perturbation.[26] We clarified the thermodynamic parameters

and their values based on the temperature-dependence of the thermally backward reaction for three types of BF_2DBM derivatives having *tert*-butyl (*t*-Bu) and methoxy (MeO) groups, two *tert*-butyl groups, and dimethoxy groups. That study revealed for the first time that the formation of the transition state was governed by both enthalpic ($\Delta H^{\ddagger}$) and entropic ($\Delta S^{\ddagger}$) terms and the activation energy of the reactions is controlled by the substituents. The data suggested that the mechanochromism could be controlled by $\Delta S^{\ddagger}$ depending on the substituents. Thermodynamically, $\Delta S^{\ddagger}$ functions as an indicator of the sterical state and order of species. However, the entropy does not generally impact the overall chemical reaction, especially in solution. The kinetics of the mechanofluorochromism of BF_2DBM derivatives is governed not only by intermolecular interactions assisted by substituent groups, but also by the molecular order in the solid state, as revealed by temperature-dependent fluorescence changes. It is important to evaluate thermodynamic properties of the materials based on the phase transformation to design the smart molecules.

In this study, the thermally backward reaction associated with the mechanofluorochromism of BF_2DBM derivatives, accompanied by an amorphous–crystalline phase transition, is quantitatively evaluated by analysis of the kinetics and thermodynamics of the transition state. The differences in the amorphous–crystalline phase depending on the substituents are also evaluated. The kinetics of the mechanofluorochromism is discussed based on the reaction coordinates, which are in turn discussed based on the thermodynamic parameters [$\Delta H^{\ddagger}$, $\Delta S^{\ddagger}$, and Gibbs energy ($\Delta G^{\ddagger}$)]. The thermodynamic parameters are determined by evaluating the effects of temperature on the time-dependent changes of the fluorescence intensity of the amorphous samples induced by mechanical grinding. The thermodynamics of the amorphous–crystalline phase transition are discussed based on data obtained by differential scanning calorimetry (DSC).

Experimental

The molecular structures of the BF_2DBM derivatives are shown in Chart 1. In this study, we used 1-(4-*tert*-butylphenyl)-3-(4-methoxyphenyl)-1,3-propanedione (**ab**), 1,3-bis(4-methoxyphenyl)-1,3-propanedione (**2a**), 1,3-bis(4-*tert*-butylphenyl)-1,3-propanedione (**2b**), 1,3-bis(4-isopropylphenyl)-1,3-propanedione (**2c**), and 1,3-bis(4-ethylphenyl)-1,3-propanedione (**2d**) as ligands. Ligands **2c** and **2d** were synthesized according to previous reports.[23, 27, 28] Boronation was performed by addition of $BF_3 \cdot OEt_2$ in CH_2Cl_2 according to a previous report.[10] Purification was carried out via column chromatography. A 2.0×10^{-3} mol·dm^{-3} CH_2Cl_2 solution of the BF_2DBM complexes was dropped on paraffin-coated weighing paper (2×2 cm) and the solvent-evaporated sample was then used for spectroscopic studies, the samples of which are uniformed fluorescence properties regardless of annealing. Fluorescence spectra were recorded on a Shimadzu RF-5300PC fluorescence spectrophotometer. In order to apply a mechanical perturbation to the BF_2DBM complexes, the

samples were rubbed with a spatula; because the smearing of samples performed in inside a sample compartment of the fluorescence spectrometer due to determine the time origin after smearing more precisely. In order to confirm the applied smearing force by the spatula was measured by using a force gauge (Imada ZTS-200N) with a cone-shaped attachment (Imada S-3). The temperature around the sample was controlled with a home-made system using a rubber heater (Hakko) and digital temperature controller (Omron E5CN-QT). Differential Scanning Calorimetry (DSC) analysis was performed by using either a SII Exstar6000 DSC6220 or a RIGAKU DSC8230 instrument. Alumina (Al_2O_3) was used as a standard material; the elevation velocity was set to 5 K·min^{-1}. The respective sample quantities were 3 mg for **abBF$_2$**, **2cBF$_2$**, and **2dBF$_2$** and 5 mg for **2aBF$_2$** and **2bBF$_2$**.

abBF$_2$: X = OMe, Y= *t*-Bu
2aBF$_2$: X = Y = OMe
2bBF$_2$: X = Y = *t*-Bu
2cBF$_2$: X = Y = *i*-Pr
2dBF$_2$: X = Y = Et
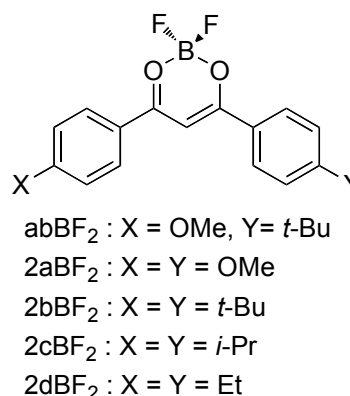
Chart. 1 Molecular structures of BF_2DBM derivatives.

Results and Discussion

Quantitative evaluation of mechanical smearing for the fluorescence spectral changes of BF_2DBM derivatives

We previously reported the mechanofluorochromic properties of BF_2DBM derivatives in a communication.[26] The drop-casted **abBF$_2$** powder exhibited blue emission with a maximum at 460 nm. The fluorescence spectrum originated from the cyan crystal as previously observed.[10] After rubbing the sample with a spatula, a new fluorescence band appeared around 500 nm with a shoulder at 550 nm, originating from the amorphous state of **abBF$_2$**. For semi-quantitative evaluation of the mechanical perturbation, the applied force (shear load) on the BF_2DBM derivatives was checked by using a force gauge.

Fig. 1a shows the fluorescence spectra of **abBF$_2$** on paraffin-coated weighing paper at 303 K as a function of smearing time at constant shear load (0.58 N). The fluorescence spectra were normalized to the maximum intensity. The fluorescence intensity around 550 nm was proportional to the smearing time, as shown in Fig. 1b. Fig. 1c shows changes in the fluorescence spectra of **abBF$_2$** as a function of perturbation for 25 s by applying various degrees of force. The relative fluorescence intensity increased linearly with increasing applied force, as shown in Fig. 1d. Using this plot, the mechanical force applied by the spatula was evaluated to be about 0.78 N for a constant time of 25 s. This is the groundbreaking demonstration that the force-dependent

fluorescence changes can be treated quantitatively.
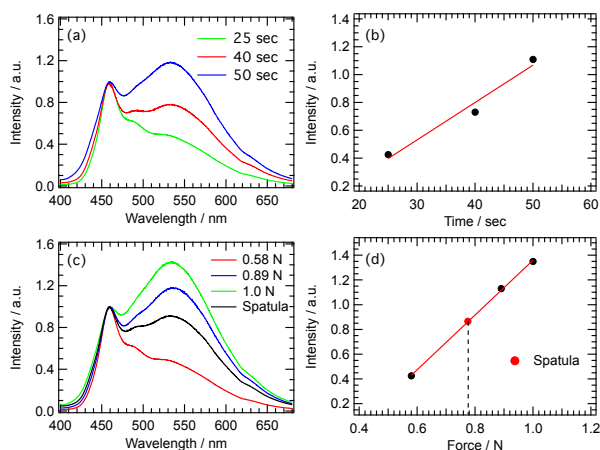
Fig. 1 Fluorescence spectra of **abBF$_2$** as a function of time for application of constant force (a, b) and applied force for a constant time of 25 s (c, d). The closed circles indicate relative fluorescence intensity at 550 nm.

Effect of substituent on rate of thermally backward reaction of BF$_2$DBM derivatives

In a prior communication, we reported the thermally backward reaction of **abBF$_2$**, **2aBF$_2$**, and **2bBF$_2$**.[26] After rubbing, the samples exhibited yellow-green emission under UV irradiation. The fluorescence intensity at wavelengths below 530 nm decreased as time elapsed. After 1030 min, the fluorescence spectrum showed peaks around 460 and 500 nm, where the emission appeared green under UV irradiation. These observations indicated that the yellow fluorescing species changed to green emitting species at room temperature, demonstrating that BF$_2$DBM derivatives act as t-type mechanochromic molecules.

The thermally backward reaction was strongly affected by the substituent on the BF$_2$DBM derivative, as reported previously.[26] We examined the substituent-dependence of the rate constants of the thermally backward reaction subsequent to mechanical perturbation. Changes in the fluorescence intensity were monitored in order to conduct a quantitative kinetic analysis of the thermally backward reaction after mechanical perturbation. Fig. 2 shows fluorescence spectra of the BF$_2$DBM derivative before and after the moment of smearing. In the case of **2aBF$_2$** (Fig. 2a), a fluorescence peak was observed around 490 nm. Build-up of a new broad emission band around 550 nm was observed after smearing the molecules. The intensity of the fluorescence peak around 550 nm decreased with the elapse of time. The fluorescence peak shifted to the red region (around 550 nm) after smearing in the case of **2bBF$_2$** (Fig. 2b); this change is largely similar to that observed for **2aBF$_2$**. Relatively small changes, such as broadening of the spectra in the wavelength range of 520 to 600 nm, were observed in the case of **2cBF$_2$** and **2dBF$_2$**, as shown in Figs. 2c and 2d, respectively.

Fig. 3 shows the changes in the fluorescence intensity of the samples at 550 nm as a function of time after mechanical perturbation; the excitation wavelength was 370 nm. The temperature was maintained constant during the measurement, as indicated in each part of Fig. 3. The fluorescence intensity decayed exponentially following the manual smearing process. The fluorescence intensity at 550 nm decreased with elapsed time; this behavior could be reproduced with a double-exponential decay function obeying first-order kinetics. Assuming first-order kinetics for the thermally backward reaction, the rate constants of the faster (k_F) and slower (k_S) components obtained by least-squares fitting are listed in Table S1 in the ESI. Both sets of rate constants increased with increasing temperature.
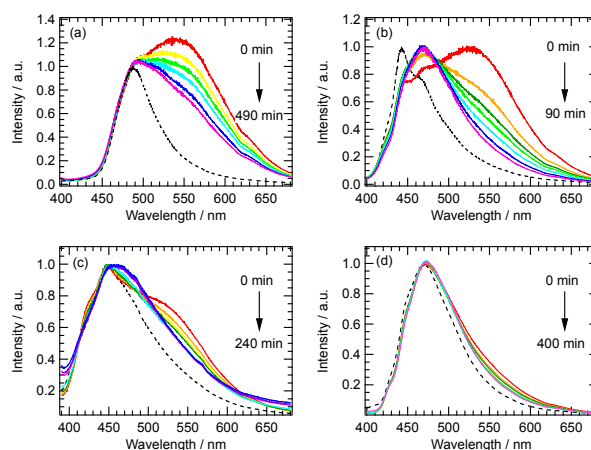
Fig. 2 Fluorescence spectra of **2aBF$_2$** (a), **2bBF$_2$** (b), **2cBF$_2$** (c), and **2dBF$_2$** (d) at 303 K. Excitation wavelength: 370 nm.
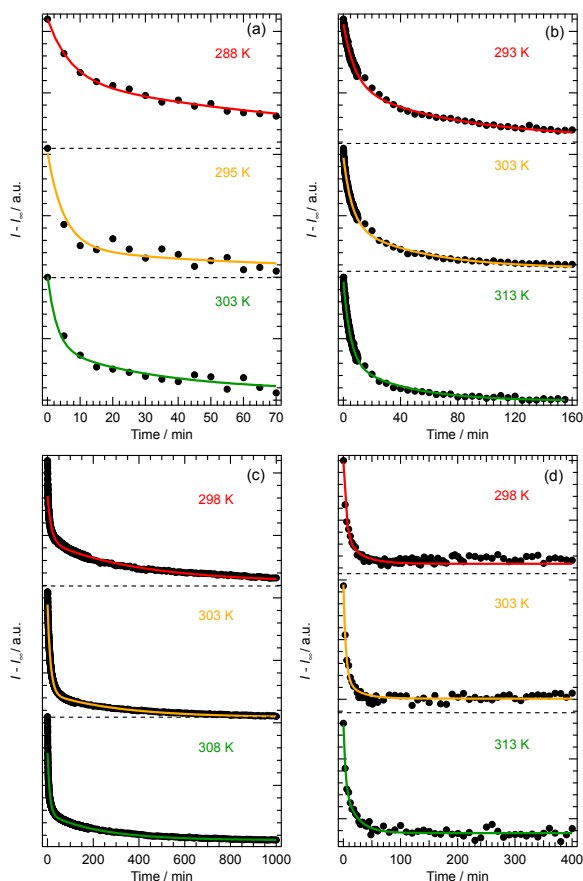
Fig. 3 Changes in fluorescence intensity of **2aBF₂** (a), **2bBF₂** (b), **2cBF₂** (c), and **2dBF₂** (d) monitored at 550 nm as a function of time after mechanical perturbation. The temperature is indicated in each profile. The solid lines indicate the best-fit curves based on a double-exponential decay function.

Thermodynamic parameters at transition state of thermally backward reaction of BF₂DBM derivatives

The thermodynamic parameters of the thermally backward reaction were estimated by using Arrhenius and Eyring plots. The temperature-dependence of the rate constants allowed us to determine the thermodynamic parameters for the mechanofluorochromism of the BF₂DBM derivatives. The Arrhenius and Eyring plots can be use to determine the pre-exponential factor (A), activation energy (E_a), and the enthalpy and entropy for activation ($\Delta H^{\ddagger}$ and $\Delta S^{\ddagger}$) of the thermally backward reaction. The left hand side of Fig. 4 shows the Arrhenius plot for the thermally backward reaction of BF₂DBM derivatives along with the straight line least-squares fitting using the following equation:

$$\ln k = \ln A - \frac{E_a}{RT} \qquad (1)$$

where R and T are the gas constant (8.314 J·K⁻¹·mol⁻¹), and temperature, respectively. The right hand side of Fig. 4 shows the Eyring plot for the thermally backward reaction of BF₂DBM derivatives along with the straight line from least-squares fitting using the following equation:

$$\ln\left(\frac{k}{T}\right) = \ln\left(\frac{k_B}{h}\right) + \frac{\Delta S^{\ddagger}}{R} - \frac{\Delta H^{\ddagger}}{RT} \qquad (2)$$

where k_B and h are the Boltzmann constant (1.380×10^{-23} J·K⁻¹) and Planck constant (6.626×10^{-34} J·s), respectively. Table 1 shows the thermodynamic parameters for the BF₂DBM derivative based on both k_F and k_S. Using **abBF₂** as an example, A and E_a were estimated to be 1.05×10^6 s⁻¹ and 45.8 kJ·mol⁻¹ for k_F, and 3.00×10^1 s⁻¹ and 27.2 kJ·mol⁻¹ for k_S. The resulting $\Delta H^{\ddagger}$ values were 43.2 kJ·mol⁻¹ for the faster component and 24.6 kJ·mol⁻¹ for the slower component, and the $\Delta S^{\ddagger}$ values were −104 J·K⁻¹·mol⁻¹ for the faster component and −191 J·K⁻¹·mol⁻¹ for the slower component.

The compounds are divided into two groups based on the E_a values for k_F [(**i**): **abBF₂** and **2aBF₂** and (**ii**): **2bBF₂**, **2cBF₂**, and **2dBF₂**], where the k_F values for group (**i**) compounds are larger than those of group (**ii**). These observations suggest that the MeO group in (**i**) affects the thermally backward reaction. The A values for k_F are much larger than of the corresponding values for k_S, meaning that the reaction probability or frequency is low for k_S. In addition, the possibility of degradation of BF₂DBM by thermal irradiation or photoirradiation, especially **2cBF₂** and **2dBF₂**, cannot be excluded. Therefore, we focus on the thermodynamic parameters obtained from k_F.

The estimated $\Delta S^{\ddagger}$ values are negative, suggesting that the order parameter of the activated complex is higher than that of the initial amorphous phase. The thermodynamic findings confirmed that the thermally backward reaction of BF₂DBM derivatives originates from the amorphous–crystalline transformation, which is described below.[10]

Both $\Delta H^{\ddagger}$ and $\Delta S^{\ddagger}$ are influenced by the substituents. The $\Delta H^{\ddagger}$ values for k_F ($\Delta H_F^{\ddagger}$) are comparable for all group (**i**) species, and are identical to the E_a; these values are twice as large as those of group (**ii**) species. All $\Delta H^{\ddagger}$ values were much larger than the energy of formation for van der Waals interactions (generally 1 kJ·mol⁻¹), but were comparable to the dipolar interaction as hydrogen bonding interaction energies (about 17–63 kJ·mol⁻¹), suggesting that the intermolecular interaction relies mainly on hydrogen-bonding to generate the transition state (activated complex).[29] The data indicate that the $\Delta H_F^{\ddagger}$ values of group (**i**) species are influenced by the MeO group, which is most probably associated with the excess energy from breaking of the C(arene)−H···O(methoxy) bond.[10, 14] The $\Delta S^{\ddagger}$ values for k_F ($\Delta S^{\ddagger}_F$) of group (**i**) were around -110 J·K⁻¹·mol⁻¹ compared with −190 J·K⁻¹·mol⁻¹ for group (**ii**). The $\Delta S^{\ddagger}_F$ of group (**i**) is larger than those of group (**ii**) by ca. 80 J·K⁻¹·mol⁻¹, suggesting that the activation complexes of (**ii**) are more ordered than those of (**i**). The Gibbs energy barriers ($\Delta G^{\ddagger}$) of BF₂DBM at 303 K are listed in Table 2. All $\Delta G^{\ddagger}_F$ values were within the range of 74.8–80.8 kJ·mol⁻¹, and were comparable for all members of the BF₂DBM series, although $\Delta H^{\ddagger}$ and $\Delta S^{\ddagger}$ around room temperature depended strongly on the substituents. Furthermore, no remarkable effect of $\Delta H^{\ddagger}$ on $\Delta G^{\ddagger}$ was recognized in the room temperature range. These findings indicate that the significant driving force for formation of the activation complex is not only $\Delta H^{\ddagger}$ but also $\Delta S^{\ddagger}$, leading to the conclusion that the substituents exert entropic control in the solid-phase reaction. It is, therefore, proposed that the substituent-dependent $\Delta S^{\ddagger}$ term is one of the key parameters influencing the mechanofluorochromism of BF₂DBM derivatives associated with the amorphous–crystalline phase
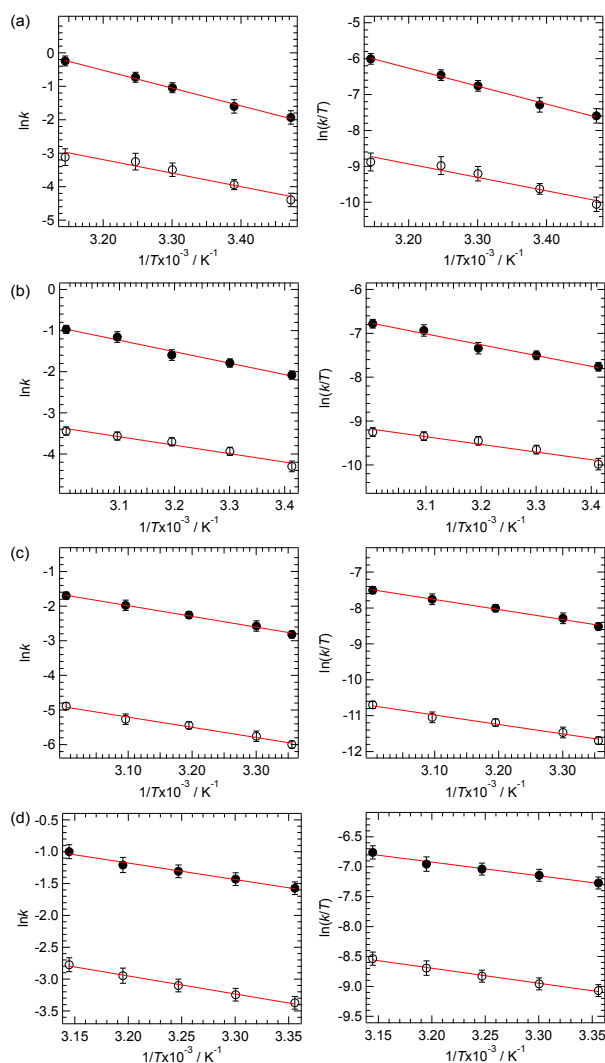
transition.

Fig. 4 Arrhenius (left side) and Eyring (right side) plots for thermally
backward reaction of **2aBF$_2$** (a), **2bBF$_2$** (b), **2cBF$_2$** (c), and **2dBF$_2$** (d).
Closed and open circles correspond to faster and slower components.

Table 1. Thermodynamic parameters at the transition state of BF$_2$DBM
derivatives

	Component	E_a / kJ·mol^{-1}	A / s^{-1}	$\Delta H^{\ddagger}$ / kJ·mol^{-1}	$\Delta S^{\ddagger}$ / J·K^{-1}·mol^{-1}
abBF$_2$	Faster	45.8	1.05×10^6	43.2	-104
	Slower	27.2	3.00×10^1	24.6	-191
2aBF$_2$	Faster	44.1	2.36×10^5	41.6	-116
	Slower	33.6	2.82×10^2	31.1	-172
2bBF$_2$	Faster	23.1	2.65×10^1	20.5	-192
	Slower	33.6	2.70×10^{-1}	14.5	-230
2cBF$_2$	Faster	25.8	3.44×10^1	23.2	-190
	Slower	23.5	8.62×10^{-1}	21.9	-221
2dBF$_2$	Faster	21.6	2.06×10^1	19.0	-194
	Slower	23.5	7.37×10^0	20.9	-203

Table 2. Gibbs energy at transition state for k_F of BF$_2$DBM derivatives

Temperature / K	$\Delta G^{\ddagger}_F$ / kJ·mol^{-1}				
	abBF$_2$	**2aBF$_2$**	**2bBF$_2$**	**2cBF$_2$**	**2dBF$_2$**
273	71.7	73.3	72.9	75.1	72.0
283	72.7	74.4	74.8	77.0	74.0
293	73.8	75.6	76.8	78.9	75.9
303	74.8	76.7	78.7	80.8	77.9
313	75.8	77.9	80.6	82.7	79.8

Relationship between thermodynamic parameters of the crystallization processes and the crystal packing of BF$_2$DBM derivatives

In the previous section, we investigated the thermodynamic parameters for formation of the activated complex (transition state). It is important to evaluate the thermal properties of the solid state, including the phase transformation from amorphous to crystal in the present type of mechanofluorochromism. In order to clarify the effects of substitution on the thermodynamic parameters for the crystallization process, DSC curves were acquired. Fig. 5 shows the DSC curves of the BF$_2$DBM derivatives. In the case of **abBF$_2$**, an exothermic peak around 433 K and endothermic peak 513 K were observed in the heating cycle and an exothermic peak around 441 K was observed in the cooling cycle. The small exothermic peak observed around 433 K most plausibly originated from phase transformation of a small amount of the blue-emitting phase to the green-emitting phase in **abBF$_2$** due to polymorphism. The peaks around 513 and 433 K originated from the melting and crystallization of **abBF$_2$**, respectively. Endothermic peaks corresponding to the melting points (T_m) were observed around 508, 545, 486, and 477 K for **2aBF$_2$**, **2bBF$_2$**, **2cBF$_2$**, and **2dBF$_2$**, respectively. Exothermic peaks corresponding to the crystallization temperature (T_c) were observed around 495, 519, 437, and 461K for **2aBF$_2$**, **2bBF$_2$**, **2cBF$_2$**, and **2dBF$_2$**, respectively. We estimated the enthalpy (ΔH_c) and entropy (ΔS_c) of crystallization based on the peak area of the DSC curves and by using the equation: $\Delta H_c = T\Delta S_c$; the resulting values are listed in Table 3. The complexes could be arranged in the following order based on both ΔH_c and ΔS_c: **2cBF$_2$** ≈ **2dBF$_2$** > **2bBF$_2$** > **abBF$_2$** ≈ **2aBF$_2$**. The value of ΔH_c depends on the intermolecular interaction. To evaluate this order, the position of short contacts of less than the summation of the van der Waals (vdW) radii of adjacent molecules in the BF$_2$DBM crystals were estimated based on X-ray crystallography. Boron difluoride, as a coordinate, interacts with two phenyl rings of other molecules. In addition, in the case of **abBF$_2$** and **2aBF$_2$**, short contact with the boron difluoride coordinate does not only occur with the two phenyl-rings, but also with the MeO group. Notably, ΔS_c is strongly affected by the intermolecular interaction with the MeO group. This leads to the conclusion that this interaction preferentially promotes crystal reformation and can contribute not only to the C(arene)−H⋯F interaction[30], but also to rotational motion around the C−O group. Recently, Sket et al. reported that the rotation around the C−O bond of a DBM-substituted dimethoxy group resulted in the formation of two polymorphs because of the low energy barrier.[31] The degree of freedom of

the molecular motion in BF_2DBM derivatives containing the MeO group will be high; consequently, it can be considered that the entropy values become large. These findings are consistent with the substituent-dependence of the thermodynamic parameters of the BF_2DBM complexes. External stimuli may thus promote the activation of rotational motion around the C−O bonds. Therefore, it is suggested that the entropic term can control the crystal formation process based on the substituents.
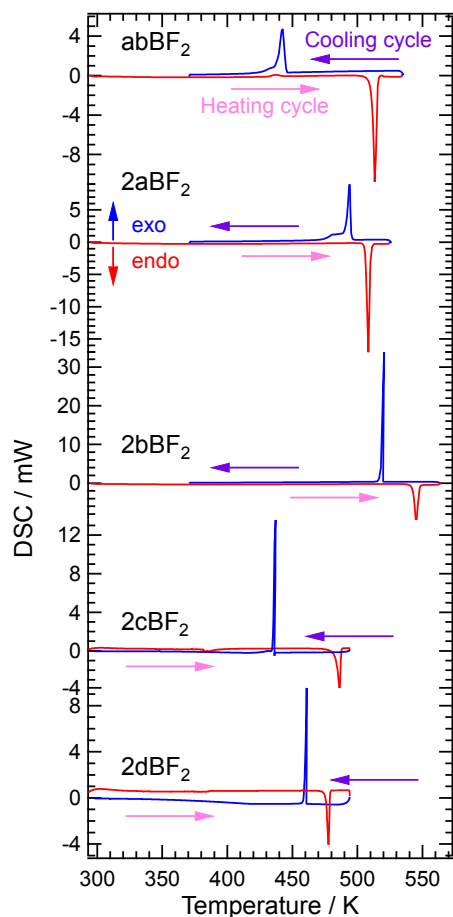
Fig. 5 DSC curves of **abBF₂**, **2aBF₂**, **2bBF₂**, **2cBF₂**, and **2dBF₂**.

The Gibbs energy of crystallization (ΔG_c) was then estimated by $\Delta G_c = \Delta H_c - T\Delta S_c$, the values of which are summarized in Table 4. The complexes can be arranged in the following order based on their ΔG_c values: **2cBF₂ ≈ 2dBF₂ > 2bBF₂ ≈ abBF₂ ≈ 2aBF₂**; this order differs from those based on ΔH_c and ΔS_c. The stacking properties of the BF_2DBM derivatives depend on the substituent structure, as reported previously.[23, 28] The overlap between adjacent molecules in crystals with face-to-face orientation can be divided into two groups: overlap between benzene (B) and dihydrodioxaborinine (D) rings (termed B-on-D overlap) and overlap between two benzene rings (B-on-B overlap) based on X-ray crystallographic analyses.[23] The molecules in crystals of **abBF₂**, **2aBF₂**, and **2bBF₂** are aligned in the B-on-D overlap mode, while those in **2cBF₂** and **2dBF₂** are aligned in

the B-on-B overlap mode, as shown in the inset of Fig. 6. These findings suggest that ΔG_c is dependent on the molecular packing mode in the crystal and is governed by a balance between the ΔH_c and ΔS_c values. It is proposed that a higher degree of overlap results in stronger intermolecular interactions, such as π–π interaction, which helps to explain the solid-state fluorescence properties of BF_2DBM derivatives.[23, 27, 28]

Table 3. Thermodynamic parameters for crystallization of BF_2DBM derivatives

	T_c / K	ΔH_c / kJ·mol⁻¹	ΔS_c / J·K⁻¹·mol⁻¹
abBF₂	445	−33.8	−76.0
2aBF₂	495	−33.5	−67.7
2bBF₂	519	−25.8	−49.8
2cBF₂	437	−13.6	−31.1
2dBF₂	461	−11.6	−25.2

Table 4. Gibbs energy of crystallization of BF_2DBM derivatives

Temperature / K	ΔG_C / kJ·mol⁻¹				
	abBF₂	**2aBF₂**	**2bBF₂**	**2cBF₂**	**2dBF₂**
273	−13.1	−15.0	−12.2	−5.1	−4.7
283	−12.3	−14.3	−11.7	−4.8	−4.5
293	−11.5	−13.7	−11.2	−4.5	−4.2
303	−10.8	−13.0	−10.7	−4.2	−4.0
313	−10.0	−12.3	−10.2	−3.9	−3.7

Reaction coordinates for mechanofluorochromism of BF_2DBM derivatives based on thermodynamic evaluation

Based on these findings, we present a schematic representation of the reaction coordinates of the thermally backward reaction of BF_2DBM derivatives in Fig. 6. These values are estimated at the temperature of 303 K. Both $\Delta H^\ddagger$ and $\Delta S^\ddagger$ are strongly dependent on the substituents, although the $\Delta G^\ddagger$ values are comparable for all BF_2DBM derivatives at 303 K, indicative of compensation between the enthalpy and the entropy. These findings indicate that the substituent group of the BF_2DBM derivatives does not affect the energy barrier for the system, but does affect the rate of the thermally backward reaction. Comparison of these values with those of **abBF₂** shows that $\Delta G^\ddagger$ is not dependent on the substituent group. Formation of the activated complex (transition state) is governed by the entropic term. The $\Delta H^\ddagger$ value is much larger than the energy of formation of van der Waals interactions (generally 1 kJ·mol⁻¹), but is comparable to the energy of dipolar and hydrogen bonding interactions (10–150 kJ·mol⁻¹).[29] Notably, the $\Delta H^\ddagger$ values obtained with the MeO groups are larger than obtained with the alkyl groups. It is proposed that the MeO groups facilitate rotational motion around the C−O group.[31]

Fraser et al. suggested that multiple interactions, such as strong dipolar interactions of the molecules, arene stacking, and C(phenyl)−H⋯F hydrogen bonds, may be the driving forces for aggregation of the BF_2DBM derivatives upon thermal treatment or recovery after smearing.[10] Because the kinetic mode related to the MeO groups preferentially promotes crystal reformation, the driving force and formation of a transition state during crystallization of BF_2DBM

derivatives will contribute not only to the C(phenyl)−H···F interaction, but also to rotational motion around the C(methyl)−O group.[32] These findings strongly suggest that the mechanofluorochromism of BF_2DBM derivatives is governed by the substituent groups that influence the entropic-dominated process (in terms of the kinetic and the thermodynamic parameters) for the thermally backward reaction. It is proposed that the reaction dynamics of **2aBF₂** is governed by either an electrostatic interaction between the H[−C(phenyl)] and O(methoxy) groups or rotational motion around the C(methyl)−O bond.
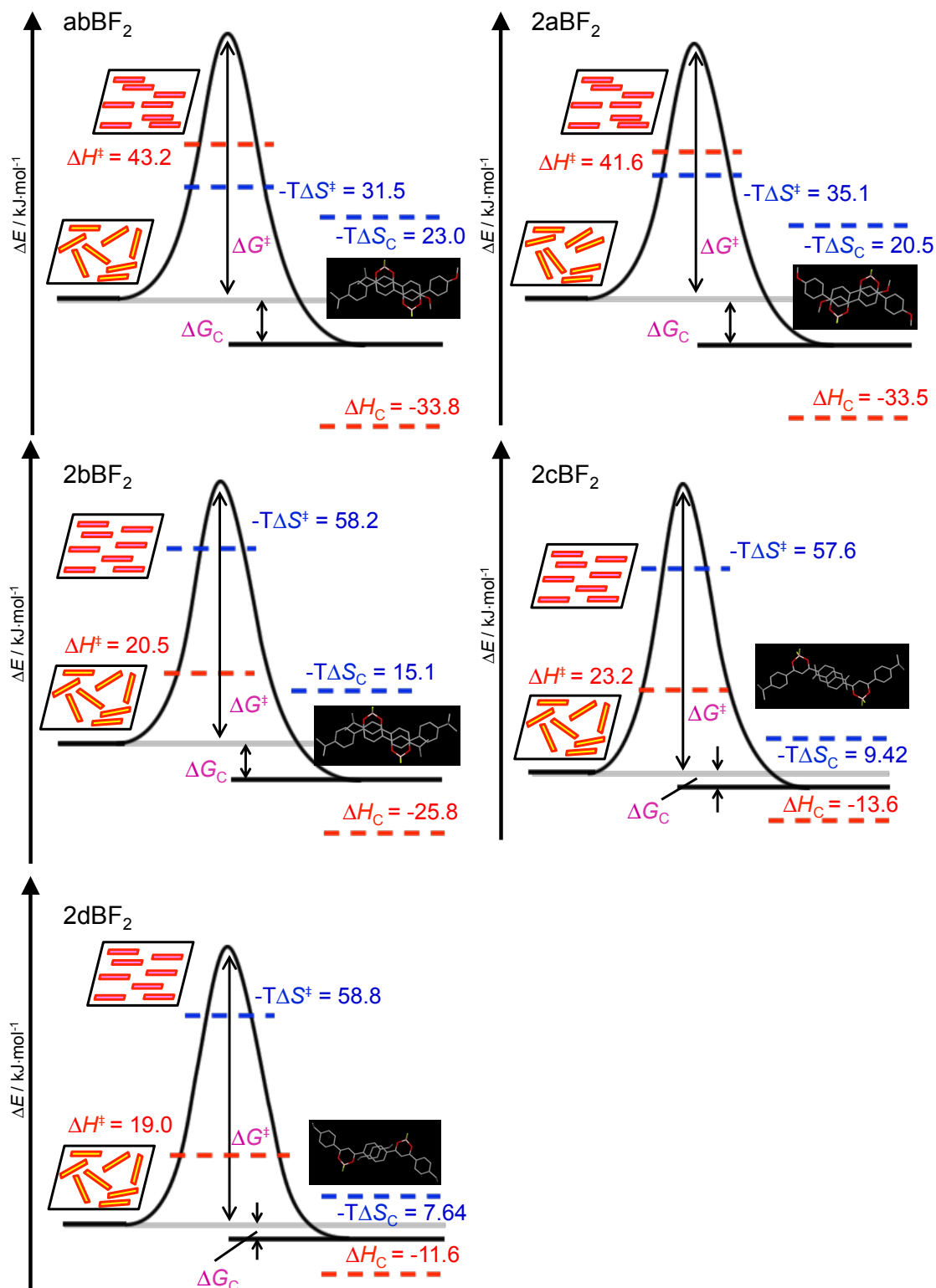
Fig. 6 Schematic representation of thermally backward reaction coordinates of BF$_2$DBM derivatives showing thermodynamic parameters at 303 K and molecular packing obtained by X-ray crystallography.

Conclusions

The thermodynamic parameters for the thermally backward reaction of BF$_2$DBM derivatives after mechanical perturbation were strongly dependent on the substituents. The substituent groups affect not only the mode of molecular packing or stacking in the crystals, but also the thermodynamic parameters in the transition states. The activation parameters for the amorphous–crystalline phase transition suggested that the energy of the transition state of the activated complex was higher than that of the initial amorphous phase based on the negative $\Delta S^{\ddagger}$ values. Although the $\Delta H^{\ddagger}$ values depend on the substituents, the $\Delta G^{\ddagger}$ values are comparable within the range of ambient temperature. It is proposed that the $\Delta S^{\ddagger}$ terms for the thermally backward reaction are governed by the solid-phase reaction, i.e., the amorphous–crystalline transformation controlled by the substituent groups. It is, therefore, suggested that the substituent-dependent $\Delta S^{\ddagger}$ term is one of the key parameters for understanding the mechanofluorochromism of BF$_2$DBM derivatives associated with the amorphous–crystal phase transition. The substituent groups influence the rate of the thermally backward reaction, where the reaction rate is most plausibly controlled by intermolecular interactions such as hydrogen bonding between the BF$_2$DBM derivatives as well as their rotational motion. On the other hand, ΔG_{C} is dependent on the molecular packing mode in the crystal, meaning that a higher degree of overlap results in stronger intermolecular interactions, such as π–π interaction. These findings should aid in the design of mechanofluorochromic reactions through judicious selection of the substituent groups, and also influence studies on the kinetics and thermodynamics of the formation of crystal nuclei upon transition from a melted state to a crystal state. Furthermore, these findings open an avenue for fabrication of organic optoelectronic materials based on the crystalline-to-amorphous transition. Thermodynamic studies of the amorphous-crystalline transformation will be useful for molecular design of organic molecular solids. The surface and substrate effects are important to develop the materials, which will be the subject of further study.

Acknowledgements

Notes and references

[a] Department of Chemistry, Institute of Education, Shinshu University, 6-ro, Nishinagano, Nagano 380-8455, Japan. Fax: +81-26-238-4114; Tel: +81-26-238-4114; E-mail: fito@shinshu-u.ac.jp;
[b] Department of Applied Chemistry, Graduate School of Engineering, Osaka Prefecture University, 1-1 Gakuen-cho, Naka-ku, Sakai, Osaka 599-8531, Japan
[c] Department of Applied Chemistry, Faculty of Engineering, Kyushu University, 744 Motooka, Nishi-ku, Fukuoka 819-0395, Japan

1   Z. G. Chi, X. Q. Zhang, B. J. Xu, X. Zhou, C. P. Ma, Y. Zhang, S. W. Liu and J. R. Xu, *Chem. Soc. Rev.*, 2012, **41**, 3878-3896.
2   Y. Sagara and T. Kato, *Nat. Chem.*, 2009, **1**, 605-610.
3   Y. Sagara, S. Yamane, T. Mutai, K. Araki and T. Kato, *Adv. Funct. Mater.*, 2009, **19**, 1869-1875.
4   Y. Sagara and T. Kato, *Angew. Chem. Int. Ed.*, 2008, **47**, 5175-5178.
5   Y. Ooyama, G. Ito, H. Fukuoka, T. Nagano, Y. Kagawa, I. Imae, K. Komaguchi and Y. Harima, *Tetrahedron*, 2010, **66**, 7268-7271.
6   J. Ni, X. Zhang, N. Qiu, Y. H. Wu, L. Y. Zhang, J. Zhang and Z. N. Chen, *Inorg. Chem.*, 2011, **50**, 9090-9096.
7   Y. Sagara, T. Mutai, I. Yoshikawa and K. Araki, *J. Am. Chem. Soc.*, 2007, **129**, 1520-1521.
8   Y. A. Lee and R. Eisenberg, *J. Am. Chem. Soc.*, 2003, **125**, 7778-7779.
9   H. Ito, T. Saito, N. Oshima, N. Kitamura, S. Ishizaka, Y. Hinatsu, M. Wakeshima, M. Kato, K. Tsuge and M. Sawamura, *J. Am. Chem. Soc.*, 2008, **130**, 10044-10045.
10 G. Q. Zhang, J. W. Lu, M. Sabat and C. L. Fraser, *J. Am. Chem. Soc.*, 2010, **132**, 2160-2162.
11 W. A. Morris, T. D. Liu and C. L. Fraser, *J. Mater. Chem. C*, 2015, **3**, 352-363.
12 T. Liu, A. D. Chien, J. Lu, G. Zhang and C. L. Fraser, *J. Mater. Chem.*, 2011, **21**, 8401-8408.
13 G. Q. Zhang, J. P. Singer, S. E. Kooi, R. E. Evans, E. L. Thomas and C. L. Fraser, *J. Mater. Chem.*, 2011, **21**, 8295-8299.
14 X. X. Sun, X. P. Zhang, X. Y. Li, S. Y. Liu and G. Q. Zhang, *J. Mater. Chem.*, 2012, **22**, 17332-17339.
15 N. D. Nguyen, G. Q. Zhang, J. W. Lu, A. E. Sherman and C. L. Fraser, *J. Mater. Chem.*, 2011, **21**, 8409-8415.
16 S. P. Xu, R. E. Evans, T. D. Liu, G. Q. Zhang, J. N. Demas, C. O. Trindle and C. L. Fraser, *Inorg. Chem.*, 2013, **52**, 3597-3610.
17 A. G. Mirochnik, E. V. Fedorenko, T. A. Kaidalova, E. B. Merkulov, V. G. Kulyavyi, K. N. Galkin and V. E. Karasev, *J. Lumin.*, 2008, **128**, 1799-1802.
18 M. Halik, W. Wenseleers, C. Grasso, F. Stellacci, E. Zojer, S. Barlow, J. L. Bredas, J. W. Perry and S. R. Marder, *Chem. Commun.*, 2003, 1490-1491.
19 E. Cogne-Laage, J. F. Allemand, O. Ruel, J. B. Baudin, V. Croquette, M. Blanchard-Desce and L. Jullien, *Chem. Eur. J.*, 2004, **10**, 1445-1455.
20 K. Ono, K. Yoshikawa, Y. Tsuji, H. Yamaguchi, R. Uozumi, M. Tomura, K. Taga and K. Saito, *Tetrahedron*, 2007, **63**, 9354-9358.
21 G. Zhang, J. Chen, S. J. Payne, S. E. Kooi, J. N. Demas and C. L. Fraser, *J. Am. Chem. Soc.*, 2007, **129**, 8942-8943.
22 J. Samonina-Kosicka, C. A. DeRosa, W. A. Morris, Z. Y. Fan and C. L. Fraser, *Macromolecules*, 2014, **47**, 3736-3746.
23 A. Sakai, E. Ohta, Y. Yoshimoto, M. Tanaka, Y. Matsui, K. Mizuno and H. Ikeda, *Chem. Eur. J.*, 2015, **21**, 18128-18137.
24 K. Mutoh and J. Abe, *Phys. Chem. Chem. Phys.*, 2014, **16**, 17537-17540.
25 K. Shima, K. Mutoh, Y. Kobayashi and J. Abe, *J. Phys. Chem. A*, 2015, **119**, 1087-1093.
26 F. Ito and T. Sagawa, *RSC Adv.*, 2013, **3**, 19785-19788.
27 A. Sakai, M. Tanaka, E. Ohta, Y. Yoshimoto, K. Mizuno and H. Ikeda, *Tetrahedron Lett.*, 2012, **53**, 4138-4141.
28 M. Tanaka, E. Ohta, A. Sakai, Y. Yoshimoto, K. Mizuno and H. Ikeda, *Tetrahedron Lett.*, 2013, **54**, 4380-4384.

29 T. Steiner, *Angew. Chem. Int. Ed.*, 2002, **41**, 48-76.
30 X. Zhang, C.-J. Yan, G.-B. Pan, R.-Q. Zhang and L.-J. Wan, *J. Phys. Chem. C*, 2007, **111**, 13851-13854.
31 P. Galer, R. C. Korosec, M. Vidmar and B. Sket, *J. Am. Chem. Soc.*, 2014, **136**, 7383-7394.
32 R. Davis, N. S. S. Kumar, S. Abraham, C. H. Suresh, N. P. Rath, N. Tamaoki and S. Das, *J. Phys. Chem. C*, 2008, **112**, 2137-2146.